Crystal Structures of *Escherichia coli* Dihydrofolate Reductase: The $NADP^+$ Holoenzyme and the Folate·$NADP^+$ Ternary Complex. Substrate Binding and a Model for the Transition State†

Christopher Bystroff,‡ Stuart J. Oatley,§ and Joseph Kraut*
Department of Chemistry, University of California, San Diego, La Jolla, California 92093
Received September 22, 1989; Revised Manuscript Received November 16, 1989

ABSTRACT: The crystal structure of dihydrofolate reductase (EC 1.5.1.3) from *Escherichia coli* has been solved as the binary complex with $NADP^+$ (the holoenzyme) and as the ternary complex with $NADP^+$ and folate. The Bragg law resolutions of the structures are 2.4 and 2.5 Å, respectively. The new crystal forms are nonisomorphous with each other and with the methotrexate binary complex reported earlier [Bolin, J. T., Filman, D. J., Matthews, D. A., Hamlin, R. C., & Kraut, J. (1982) *J. Biol. Chem. 257*, 13650–13662]. In general, $NADP^+$ and folate binding conform to predictions, but the nicotinamide moiety of $NADP^+$ is disordered in the holoenzyme and ordered in the ternary complex. A mobile loop (residues 16–20) involved in binding the nicotinamide is also disordered in the holoenzyme. We report a detailed analysis of the binding interactions for both ligands, paying special attention to several apparently strained interactions that may favor the transition state for hydride transfer. Hypothetical models are presented for the binding of 7,8-dihydrofolate in the Michaelis complex and for the transition-state complex.

Dihydrofolate reductase (DHFR)[1] catalyzes the NADPH-dependent reduction of 7,8-dihydrofolate to 5,6,7,8-tetrahydrofolate. Interest in this enzyme stems in part from its role as the target for antibacterial [trimethoprim (TMP)], anticancer [methotrexate (MTX)], and other clinically useful drugs. The crystal structure of *Escherichia coli* DHFR was solved and refined to high resolution in this laboratory as the binary complex with methotrexate (Matthews et al., 1977; Filman et al., 1982; Bolin et al., 1982). On the basis of that structure, hypotheses were proposed regarding the functional role of its various features [see reviews by Blakley (1984), Blakley and Appleman (1986), and Kraut and Matthews (1987)]. Since then, site-directed mutagenesis studies (Villafranca et al., 1983; Howell et al., 1986, 1987; Benkovic et al., 1988) have helped to identify specific contributions by selected side chains to catalysis, a full kinetic mechanism has been published (Fierke et al., 1987), and a low-resolution crystallographic study of the trimethoprim·NADPH ternary complex has yielded evidence for significant conformational flexibility (Champness et al., 1986). A large amount of kinetic and spectroscopic evidence from solution studies has pointed to the mechanistic importance of conformational changes on ligand binding [summarized by Kraut and Matthews (1987)]. Our overall strategy for better delineating these phenomena, and the role of conformational flexibility in DHFR function generally, is to determine accurate three-dimensional structures of the *E. coli* and other species of DHFR in various ligation states. Ultimately, we hope to arrive at a dynamical picture of how the enzyme binds its substrates, moves protons, stabilizes the transition state of the hydride-transfer reaction, and releases products.

This is the first of two reports describing three new crystal structures of *E. coli* DHFR in variously ligated states. Coordinate sets for each have been deposited with the Brookhaven Protein Data Bank. The structures of four distinct crystal forms of the *E. coli* enzyme have now been solved and refined to at least an intermediate resolution (2.5 Å or better, *R* factor less than 25%) (see Table I). The three new structures and their space groups are (1) the $NADP^+$ holoenzyme, $P2_12_12_1$, (2) the folate·$NADP^+$ ternary complex, $P3_221$, and (3) the apoenzyme, $P3_121$. The ternary complex is isomorphous with the trimethoprim·NADPH ternary complex of Champness et al. (1986), mentioned above. The $P6_1$ MTX binary complex remains the best crystal form with respect to diffraction quality.

This paper focuses on the holoenzyme and the folate·$NADP^+$ ternary complex. It describes how the enzyme binds $NADP^+$ and folate and compares the latter with the binding of MTX. We also point to enzyme–ligand interactions that may account for the enzyme's affinity for the transition state of the hydride-transfer reaction. These binding interactions are presented mainly from a static point of view, but in a later report (to be submitted for publication) we will introduce the structure of apo-DHFR and discuss ligand-induced conformational changes in the enzyme. Cooperative induction of certain conformational shifts will be proposed, and the possible role of cooperativity and conformational flexibility in transition-state binding will be discussed.

Materials and Methods

Purification of DHFR and Preparation of Complexes. Wild-type *E. coli* DHFR was purified from an overproducing SK383 strain of *E. coli* containing the plasmid pUC8 carrying the wild-type DHFR gene. Starter cultures were grown for

† This work, part of the Ph.D. dissertation of C.B., was funded by NIH Grant CA 17374. C.B. was supported by USPHS Predoctoral Training Grant 2T32 GM 07313-12.
* Author to whom correspondence should be addressed.
‡ Present address: Department of Biochemistry and Biophysics, University of California, San Francisco, CA 94143-0448.
§ Deceased April 29, 1988. We dedicate this paper to our departed friend and colleague.

[1] Abbreviations: ADP, adenosine 2′,5′-diphosphate; DHFR, dihydrofolate reductase; MTX, methotrexate; NADP(+/H), nicotinamide adenine dinucleotide (oxidized/reduced); NMN, nicotinamide mononucleotide; PABG, *N*-(*p*-aminobenzoyl)-L-glutamate; TMP, trimethoprim.

0006-2960/90/0429-3263$02.50/0

Table I: Existing *E. coli* DHFR Crystals

complex	space group	cell dimensions (Å)				pH	data (Å)	*R* factor (%)	footnote
		a	*b*	*c*					
apo	$P3_121$	68.7	68.7	83.5		5.4	2.3	19.2	*a, b*
MTX (2 molecules/asymmetric unit)	$P6_1$	93.1	93.1	73.9		6.8	1.7	15.5	*c*
TMP (2 molecules/asymmetric unit)		93.1				6.8	1.7	15.5	*d*
$NADP^+$	$P2_12_12_1$	34.8	59.0	81.3		7.0	2.4	19.8	*e, a*
TMP·NADPH	$P3_221$	61.8	61.8	105.8		6.8	3.0	44	*f*
folate·$NADP^+$		62.2	62.2	105.5		6.0	2.5	24.5	*e, a*
MTX·$NADP^+$						6.0	none		*a, g*
NADPH		62.0	62.0	107.7		7.0	none		*a*
MTX·NADPH						7.0	none		*a, g*
5-deazafolate·NADPH						7.0	none		*a, g*
folate·$NADP^+$	$P2_12_12_1$	35.7	47.7	102.2		7.0	none		*a*
$NADP^+$	$C2$	75.0	59.3	38.8	$\beta = 106°$	7.1	none		*a*

[a] Crystals grown and characterized by C.B. [b] To be submitted for publication. [c] Matthews et al. (1977), Bolin et al. (1982), and Filman et al. (1982). [d] Matthews et al. (1985). [e] This work. $P3_221$ form was solved independently of the isomorphous crystal form of Champness et al. (1986). [f] Champness et al. (1986). [g] Cell dimensions not measured directly; assumed same as the above.

about 24 h in a yeast extract/bactotryptone (YT) medium containing 200 μg/mL ampicillin and 200 μg/mL trimethoprim. Cells were washed once in sterile YT before inoculating 10–12 L of sterile YT medium containing 200 μg/mL ampicillin but no trimethoprim. DHFR was purified by the method of Villafranca et al. (1983). The typical yield was 100–300 mg of purified DHFR. All operations after harvesting of the cells and including crystallization were done at 4 °C.

The purified enzyme was dialyzed into 10 or 20 mM imidazole hydrochloride, pH 7.0, and concentrated in centrifuge concentrators (Centricon, by Amicon) to 40 mg/mL, as determined by absorption at 280 nm. Purified apo-DHFR was either frozen in liquid N_2 as a concentrated solution (20–40 mg/mL) in 20 mM imidazole hydrochloride, pH 7.0, or filtered through a 0.4-μm microfilter (Centrex) and stored at 4 °C in the same solution. To prevent microbial growth and oxidation without affecting the protein's ability to crystallize, 0.1 mM NaN_3 and 1 mM dithiothreitol were sometimes added.

The $NADP^+$ holoenzyme was made by adding 2–5 molar excess of solid $NADP^+$ (Sigma, disodium salt) to solutions of 20 mg/mL DHFR in 20 mM imidazole hydrochloride, pH 7.0. Holo-DHFR solutions were allowed to sit for several hours before setting up crystallization attempts.

The folate·DHFR binary complex was made by adding 1 mM solid folic acid (Sigma) to 1.0–2.0 mg/mL solutions of apo-DHFR in either 20 mM imidazole hydrochloride, pH 7.0, or 50 mM potassium phosphate, pH 8.0. The folate/DHFR solutions were allowed to sit at 4 °C for at least 12 h, then concentrated in Centricon concentrators, and rediluted in 50 mM potassium hydrogen phthalate, pH 6.0/NaOH to which a trace of folic acid had been added. Three cycles of redilution and reconcentration were used to remove excess folate and the previous buffer. To make the folate·$NADP^+$·DHFR ternary complex, a 2–5 molar excess of solid $NADP^+$ was added to the concentrated solution of folate·DHFR and allowed to sit for several hours before using.

Crystallization Conditions. Initial attempts to soak $NADP^+$ or NADPH into the original $P6_1$ MTX binary crystal form were unsuccessful and led to a search for a new crystal form that could incorporate $NADP^+$ (or NADPH) and/or folate. Several crystal forms were found, some crystallizing under almost identical conditions and all from PEG 6000 as the precipitating agent. All crystal forms except the apoenzyme required the presence of Ca^{2+}. All forms contain one molecule per asymmetric unit except for the $P6_1$ MTX binary, which has two. Table I lists the *E. coli* DHFR crystal forms obtained to date.

Crystals of the folate·$NADP^+$·DHFR or MTX·$NADP^+$·DHFR ternary complex were obtained as follows. PEG 6000 (50% (w/w); 1.5 μL) and 50 mM calcium acetate (1.5 μL) were added to 12 μL of concentrated (≈30 mg/mL) folate·$NADP^+$·DHFR ternary complex in an Eppendorf tube. The mixture was stirred gently to dissolve any transient precipitate and then spun in a microcentrifuge for 15 min. The supernatant was placed on a small plastic cover slip on a platform in a 2-mL well of a tissue culture plate (Linbro) in vapor contact with a reservoir solution of 12% (w/w) PEG 6000 and 3% ethanol in phthalate buffer. Crystals appeared in 5–10 days. This and all of the following successful crystallizations were done at 4 °C. The space group was determined to be either $P3_121$ or its enantiomorph $P3_221$, with cell dimensions $a = b = 62.21$ Å and $c = 105.53$ Å. Crystals of NADPH·DHFR, MTX·NADPH·DHFR, or 5-deazafolate·NADPH·DHFR are isomorphous with the crystals described above and were obtained under similar conditions.

Crystals of the $NADP^+$·DHFR binary (holoenzyme) complex were observed in at least two space groups, $P2_12_12_1$ and C2. An additional crystal form was morphologically distinguishable but remains uncharacterized owing to twinning problems. All three forms grew under the same crystallization conditions, although it was possible by varying certain parameters to favor the growth of one form over the others. The reduced holoenzyme (NADPH·DHFR) crystallized in neither of these forms but rather in the $P3_221$ form described above.

To obtain the $P2_12_12_1$ form of the holoenzyme, 1.5 μL of 1.0 M calcium acetate and 2.7 μL of 50% (w/w) PEG 6000 were added, stirring between additions, to 10.8 μL of 30 mg/mL $NADP^+$·DHFR in 10 mM imidazole hydrochloride, pH 7.0, buffer. A transient precipitate forms which dissolves upon stirring. The tube was spun for 15 min in a microcentrifuge to remove dust and any remaining precipitate. Crystals were grown by hanging-drop vapor diffusion against 15% (w/w) PEG 6000 in 10 mM imidazole hydrochloride, pH 7.0. Thick rod-shaped crystals measuring up to 0.2 × 0.2 × 1.0 mm^3 grew in 2 days–1 week. Buffered 15% PEG 6000 containing 0.1 M calcium acetate was added to the drop to facilitate crystal mounting. The unit cell dimensions are $a = 34.85$ Å, $b = 59.00$ Å, and $c = 81.28$ Å. There is one molecule in the asymmetric unit.

Data Collection. X-ray diffraction data for the $P2_12_12_1$ crystal form of the oxidized holoenzyme were collected to a Bragg spacing of 2.33 Å on the Mark 2 multiwire area detector developed by Xuong and co-workers (Cork et al., 1973; Xuong et al., 1985). A total of 41 396 observations were made on 7094 out of a possible 7586 reflections, an average of about

6 observations per reflection. Data were reduced by using programs provided at the facility (Anderson, 1987). The merging R factor[2] was 4.7%. Data to 2.4-Å resolution, 99.5% complete, were used in the refinement process.

X-ray data for the $P3_221$ folate·NADP$^+$ ternary complex were also collected at the San Diego multiwire diffractometer facility. This data set is essentially complete to 2.5 Å, with 68 035 observations of 8586 out of a possible 8598 reflections, or about 8 observations per reflection. The merging R factor was 4.9%. A dramatic decrease of intensities with increasing Bragg angle was immediately noticeable. This high overall temperature factor resulted in poor merging R factors at high resolution: 15% from 3 to 2.5 Å and 25% from 2.6 to 2.5 Å. A Wilson plot of data between 2.5 and 3.5 Å indicated an overall temperature factor of 45 Å^2. Further implications of this high temperature factor are discussed in the section on refinement of the ternary complex. It is noteworthy that diffraction by these crystals was initially observed out to 1.9 Å, but within 1 h after exposure to X-rays it decays to a limit of 2.4–2.5 Å. Oxidation of Cys-152, which is involved in a lattice interaction, is suspected of causing disorder resulting in the loss of high-angle diffraction. It may be that X-ray-induced radicals trigger the oxidation.

Phase Determination by Molecular Replacement. Each of the three new DHFR structures was solved by molecular replacement. The search model for both the holoenzyme and the ternary complex was molecule "2" of the *E. coli* DHFR·MTX crystal structure with NADP$^+$ inserted into the cofactor binding site so as to duplicate, insofar as possible, its geometry in the *Lactobacillus casei* MTX·NADPH ternary complex structure. Crowther's fast rotation function (Crowther, 1972), as modified by Tanaka (1977), was employed in searching for the orientation of the single molecule in the asymmetric unit of each crystal. Rotation of the model for the holoenzyme, using 10–3.5-Å data and a radius of integration of 21 Å, produced a peak value which was 7.9σ above the mean and separated from the highest non-symmetry-related peak by 1.8σ. Rotation of the same model for the ternary complex, using 10–4.0-Å data and a radius of integration of 24 Å, produced a peak which was 5.7σ above the mean and 0.9σ above the highest non-symmetry-related peak.

A set of programs to calculate the translation function were written by one of us and documented elsewhere (Bystroff, 1988). The main program calculates the "T1" function of Crowther and Blow (1967). It is well tested and has succeeded in solving at least seven structures, including those described here (Wang et al., 1990; J. F. Davies, unpublished results; D. A. Matthews, unpublished results).

Translating the oriented holoenzyme model, using reflections between 7.0 and 4.5 Å, we found a 6.1σ peak, approximately 0.8 Å thick at half-height. The peak position was verified as the solution and refined by using a local three-dimensional R-factor search, which gave a minimum of 41%. Calculating the translation function for the ternary complex resolved the ambiguity between space groups, showing three 6.1σ peaks for $P3_221$ but no peak higher than 3.0σ for $P3_121$. The solution position in $P3_221$ was verified by a local R-factor search, which gave a minimum of 45%.

Least-Squares Structure Refinement. With the results of molecular replacement as a starting model, COREL S (Sussman et al., 1977) was used for initial refinement of the holoenzyme. This program has demonstrated its ability to give a larger radius of convergence than PROLSQ in the early stages of refinement (Leslie, 1985) by allowing the user to define rigid domains within the molecule, thereby improving the data/parameter ratio. During COREL S refinement we started by refining the whole molecule as a single rigid group using 5-Å data and then divided the molecule into smaller and smaller rigid domains while increasing the number of data included. "Joints" between the domains were chosen to be the presumably flexible segments, i.e., loops at the ends of secondary structure. For the ternary complex, COREL S was used only for the initial rigid-body refinement. Thereafter, refinement was continued with the program PROLSQ (Hendrickson, 1985), which treats atoms individually. A solvent correction factor, described by Bolin et al. (1982), was applied throughout the refinement after initial refinement of the overall temperature factor.

After convergence of the structure (usually three to five cycles of refinement), we typically inspected both $F_o - F_c$ and $2F_o - F_c$ maps on a Silicon Graphics IRIS picture system running molecular modeling programs MMS (Dempsey, 1987) and FRODO (Jones, 1978). Possibly disordered side chains were identified by their low density in a $2F_o - F_c$ map. To decide whether to keep or omit weakly defined features, the atoms in question were deleted from the structure for three to five refinement cycles. Then if no positive difference density appeared at the site of the deleted atoms, those atoms were assumed to be disordered and were left out of the subsequent refinement. A total of 72 waters have been included in the holoenzyme structure, and 55 waters have been included in the ternary complex structure. Curiously, although the holoenzyme crystals were grown in 100 mM calcium acetate, no identifiable calcium ions were found.

Overlaying of the various structures was done by using Rossmann and Argos's program OVRLAP (Rossmann & Argos, 1975). When measured distances are reported between equivalent atoms in nonisomorphous crystal structures, these are based on the least-squares superpositions calculated by this program.

Results

Holoenzyme Refinement. A striking result of refining the holoenzyme was the absence of continuous density corresponding to the NMN moiety of NADP$^+$ and the nearby residues 16–20 within the Met-20 loop.[3] In the course of refinement, residues 16–20 and the NMN moiety were removed, and the resulting maps were inspected for difference density in that region. The presence of only weak and disconnected density led to the conclusion that the nicotinamide, most of its attached ribose, and residues 16–20 are disordered in the holoenzyme crystal. These atoms were omitted from further refinement cycles. Coordinates were refined for five atoms of the ribose that appeared at partial occupancy in the $2F_o - F_c$ maps (dashed bonds in Figure 2). Additionally, two positions of spherical density that persisted from cycle to cycle in the NMN binding cavity were, in the last three cycles, modeled by solvent atoms. Disordered, too, were the side chains beyond Cβ of Glu-120 and Asp-127.

Following up on the conclusion that the NMN and residues 16–20 are disordered, we inspected the maps to determine which torsion angle in the NADP$^+$ molecule might produce the observed effects. A large drop in density occurs between atoms NO5′ and NC5′, and a projection of weak but continuous density extends from one of the other phosphate oxygens (NO2P) out toward a solvent-filled space between two sym-

[2] $R_{merge} = \sum|av - obsd|/\sum av$.

[3] Residues 9–24 form a loop connecting βA to αB, which we have given the special name "Met-20 loop" because of its importance for positioning of Met-20 in the folate·NADP$^+$ ternary complex.

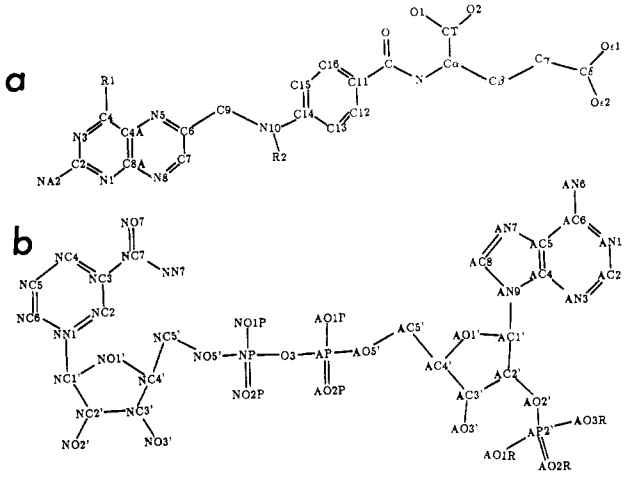

FIGURE 1: Standard atom names for (a) folate or MTX and (b) $NADP^+$. For folate, R1 = OH4 and R2 = H. For MTX, R1 = NA4 and R2 = CM.

metry-related molecules. This feature suggests that the NMN rotates 120° about the bond between the bridging pyrophosphate oxygen (O3) and the nicotinamide phosphorus (NP) so that NO5′ replaces NO2P, which projects toward the solvent-filled space, where the NMN would then rest. The NMN moiety could rotate from its bound position to a position in the solvent space without requiring any changes in the protein conformation aside from that of the partially disordered Met-20 loop. The Met-20 loop folds over the NMN binding site in the folate·$NADP^+$ ternary complex, but if this loop assumes one of the two conformations seen in the MTX binary complex, the NMN moiety would have an opening through which to rotate out of the pocket. Due to the lack of well-defined density for the nicotinamide in either of the proposed conformations, no attempt was made to refine two simultaneous positions of the NMN group. Instead, a water molecule (Wat-381) was used simply to model the density extending from NO2P. Most likely, the NMN group is rotationally disordered about its O3–NP bond with a tendency to reside preferentially in two positions. The apparent existence of two ordered solvent molecules (Wat-343, Wat-350) in the nicotinamide binding site suggests that, in the crystal, the oxidized nicotinamide ring itself spends little or no time in that site.

Refinement of the holoenzyme was stopped after 35 cycles of CORELS and 68 cycles of PROLSQ when further computation produced only insignificant improvements in either the R factor or the geometry, and difference maps did not suggest any obvious possible changes. When refinement was terminated, the R factor at 2.4 Å and 19.2%. Root mean square deviations from ideal geometry were, for bond lengths, 0.018 Å; for planar groups, they were 0.017 Å. The average temperature factor is 23 Å^2 with a standard deviation (σ) of 13 Å^2. For backbone atoms the average B is 21 Å^2, for side chains, 23 Å^2, and for ordered waters, 37 Å^2. The methoed of Luzzatti (1952) estimates an average error in atomic position of 0.30 Å.

Ternary Complex Refinement. As in the case of the holoenzyme, the $2F_o - F_c$ map near the Met-20 loop in the ternary complex initially contained disconnected density which did not correct itself without manual intervention. However, in the case of the ternary complex, modeling the backbone into $2F_o - F_c$ density was successful, resulting in improvement of the map in subsequent cycles. Residues 16–20 were modeled as a type I β-turn, similar to the type II β-turn at the same position in the *L. casei* DHFR ternary complex (Filman et al., 1982) and the same as the conformation in the isomorphous *E. coli* DHFR·TMP·NADPH ternary complex (Champness et al., 1986). Improvement of the map with refinement allowed us to then add the side chains of Asn-18 and Met-20, although the side chain of Glu-17 remains invisible.

Refinement proceeded must more slowly for the ternary complex than for the holoenzyme, and with a less satisfactory result. After 80 cycles of refinement, the final R factor is 24.5% for data between 20 and 2.5 Å. The slowness of convergence and the relatively high R factor can be attributed to the high overall temperature factor of the data, 44 Å^2 as compared to 23 Å^2 for the holoenzyme.

Disorder in the ternary complex is not confined to discrete portions of the structure, as was the case in the holoenzyme, but rather is distributed throughout the entire molecule. The average temperature factor is 44 Å^2, with σ = 10 Å^2. The average B for backbone atoms, 44 Å^2, is essentially the same as for side-chain atoms, 43 Å^2. The average B for ordered waters is 53 Å^2. A Luzzatti plot estimates the average error in atomic positions to be 0.35 Å. Although many side chains are disordered, the entire backbone and both ligands are in well-defined density. In particular, the binding sites for the pteridine and nicotinamide are well-defined regions of the map and have relatively low temperature factors (25–35 Å^2). We believe this fact justifies our detailed discussion of the interactions there. No region of the structure showed temperature factors below 22 Å^2 except for the side-chain His-114, which is involved in the lattice contact across the proper crystallographic 2-fold axis, discussed later. The uniformly high temperature factors lead us to believe that the disorder is primarily static, resulting from loose lattice interactions, and is not due to an intrinsically floppy DHFR molecule, which would display greater disorder at external loops than at internal secondary structures. In all, 10 hydrophilic side chains are either entirely or partially missing in the current model of the ternary complex structure: Glu-17, Arg-44, Glu-48, Arg-52, Arg-98, Lys-106, Asp-116, Glu-120, Glu-129, and Asp-131.

Packing Interactions. In order to separate the possible conformational effects of ligand binding from the effects of lattice interactions, we must first describe crystal packing in the various space groups. In the holoenzyme, three contacts involving six surface regions of the enzyme molecule form the $P2_12_12_1$ lattice. The $P3_221$ lattice of the ternary complex also comprises three lattice interactions, involving five regions of the molecule. In both cases a lattice interaction occurs near the Met-20 loop, which exhibits some of the largest conformational changes. More specifically, in the $P2_12_12_1$ structure a second molecule generated by an A-axis translation contacts the first molecule at the C-terminal region of the Met-20 loop (21–24) and along the F–G connecting loop (117–132). In the $P3_221$ crystal, the G–H connecting loop (143–148), paralleling the Met-20 loop and also conformationally variable, is involved in a lattice contact. Additionally, in the $P6_1$ MTX binary crystal structure the Met-20 loop is directly involved in both a lattice contact and binding of a calcium ion. Lattice interactions could explain the well-defined order observed at the Met-20 loop in that crystal structure, though the loop may be disordered in solution. Indeed, the Met-20 loop in the $P2_12_12_1$ holoenzyme structure is partially disordered in the crystal, as we have pointed out. While lattice interactions may induce order in an otherwise disordered loop, it is not easy to imagine how lattice interactions in the holoenzyme crystal could induce *disorder* in a loop that is otherwise ordered. We therefore assume that the Met-20 loop is disordered in solution in the holoenzyme complex.

An unusual symmetry-generated intermolecular disulfide bond was found at the center of a tight lattice contact in the

$P3_221$ ternary complex crystal form. A crystallographic 2-fold rotation positions Phe-140 and His-114 in one molecule to stack with His-114 and Phe-140, respectively, in another molecule, while Cys-152, located between the pairs of aromatic side chains, forms a disulfide bond with its symmetry-related partner. The significance, if any, of this symmetry-generated covalent linkage is not obvious. There is no important difference between the holoenzyme and the ternary complex in the conformation of the region surrounding Cys-152. Thus we infer that the disulfide formation does not cause any conformational differences elsewhere in the molecule. Presumably, stacking of the paired aromatic residues contributes to the dimerization energy, and the disulfide bridge forms subsequent to crystallization. Several lines of evidence suggest that this phenomenon may play a part in causing the lattice disorder seen in the $P3_221$ crystal form. Some crystal specimens of the $P3_221$ ternary complex have been observed to diffract initially to 1.9-Å resolution, but within hours they have decayed to a 2.5-Å diffraction limit. Possibly disulfide formation in the crystal is accelerated by radicals generated by the X-ray beam. The disulfide bridge may then draw the two molecules of the crystallographic dimer slightly closer together, weakening other lattice interactions and resulting in the observed high overall temperature factor.

Discussion

With the present structural solutions of two additional *E. coli* DHFR–ligand complexes, plus that of the apoenzyme, there are now available a total of five crystallographically independent views of the *E. coli* DHFR molecule (recall that the $P6_1$ MTX binary has two molecules in the asymmetric unit) in various ligations states. The new structures show that the geometry of folate and $NADP^+$ binding both conform, approximately, to the predictions of Bolin et al. (1982) and Filman et al. (1982), which were based on the MTX binary complex and the *L. casei* MTX·NADPH ternary complex. However, some significant and mechanistically important differences exist between those earlier models and the present structures, both with respect to conformation of the enzyme molecule and with respect to ligand binding geometry. In this section we will focus principally on ligand binding interactions and the question of transition-state stabilization.

A word of caution is appropriate here. Because the ternary complex structure has a somewhat high *R* factor (24.5%) and overall temperature factor (44 $Å^2$), we have endeavored to avoid giving undue significance to small deviations from standard distances for bonded and nonbonded interactions (i.e., 0.4 Å or less). But in some places several closely coupled interatomic distances deviate from ideality in a systematic fashion, lending credibility to the idea that a strained interaction is present there. The instances cited below for the possible existence of such interactions in the crystal structure never rely on the accuracy of a single distance measurement.

Overview of Conformational Differences. Although ligand-induced conformational changes will not be described in detail here, in the interest of clarity they are summarized below before continuing with a discussion of ligand binding.

The major conformational differences between the holoenzyme and the MTX binary complex occur in two places. Portions of the adenosine binding domain (approximately residues 38–88) differ by up to 2.5 Å from their position in the MTX binary, forming a larger adenosine binding crevice in the holoenzyme. And residues 16–20 in the Met-20 loop are disordered in the holoenzyme, whereas in the MTX binary they are crystallographically well ordered, although having no definable secondary structure. Other differences between these two structures are minor.

Conformational differences between the MTX binary and the folate·$NADP^+$ ternary structures also occur in the two regions mentioned above, the adenosine binding domain and the Met-20 loop, and additionally in two other places, at residues 21–28 and at residue 94. The adenosine binding domain in the ternary complex resembles the same region in the holoenzyme, again having a more open adenosine binding site. Residues 16–19 of the Met-20 loop assume a type I β-turn conformation in the ternary complex, closing over the bound nicotinamide ribose. Additionally, residues 21–24 and the αB helix, residues 25–28, are shifted up to 3 Å in the direction of the pteridine binding site in the ternary complex; and the backbone at Ile-94, bordering the pteridine binding pocket, shifts away from the bound folate in the ternary complex but toward the bound MTX in that binary complex.

Finally, conformational differences between the ternary complex and the holoenzyme occur primarily in the Met-20 loop and at the αB helix. The Met-20 loop forms a β-turn in the ternary complex but is disordered in the holoenzyme. The αB helix shifts toward the pteridine binding site in the ternary complex but occupies essentially the same position in the holoenzyme as in the MTX binary complex. Other differences between the holoenzyme and the ternary complex are probably insignificant at the current level of accuracy of the latter.

$NADP^+$ Binding. Table II lists the contacts between $NADP^+$ and the enzyme molecule. Except as noted, these interactions are the same in the holoenzyme as in the ternary complex. When discussing binding interactions with the adenosine 2′,5′-diphosphate (ADP) portion of the $NADP^+$, we will rely on the holoenzyme structure, for which the ADP region is better defined in our current electron density maps. However, when we discuss the nicotinamide mononucleotide (NMN) portion, we must rely on the ternary complex structure, as disorder of this moiety in the holoenzyme precludes analysis.

In general terms, $NADP^+$ was found to bind to *E. coli* DHFR in a mode similar to that observed for *L. casei* DHFR (Filman et al., 1982). Figure 2 shows $NADP^+$ and the binding pocket in the holoenzyme. The coenzyme is in an extended conformation, occupying a crevice that sits over the C-termini of two central β-strands: βB (38–44) and βE (90–95). These two β-strands make tight turns into helices αC (44–50) and αF (97–104), respectively, leaving H-bonding donors at the N-termini of the helices available for binding to the coenzyme. The N-terminal positive ends of the αF and αC dipoles are directed at the midpoint of the pyrophosphate and at the adenosine ribose, respectively. In the MTX binary complex, the coenzyme pocket is filled with ordered waters and two chloride ions (S. J. Oatley, unpublished data). The chlorides sit at the N-termini of the two helices—identically in both of the molecules in the asymmetric unit—approximately where the two phosphates of the pyrophosphate bridge will be accommodated in the holoenzyme.

The pyrophosphate moiety of the coenzyme appears to contribute most of the energetically favorable binding interactions with DHFR. A total of ten H-bonds, one ionic interaction (His-45), and two helix dipoles (αC and αF) stabilize the bound pyrophosphate. At least one H-bond is made to every oxygen of the pyrophosphate except the one (NO2P, also sometimes named OP2N) that is directed toward the surrounding solvent. The NO2P position was cited earlier as the possible rotated second site for NO5′ of the disordered nicotinamide ribose in the holoenzyme structure. His-45, conserved

Table II: $NADP^+$ Binding Interactions

$NADP^+$ moiety	DHFR atoms	type of interaction	comments
adenine	L62 side chain	hydrophobic	
	63–64 backbone	VDW[a]	
	76–78 backbone	VDW	
	R98 side chain	VDW	missing in ternary
	Q102 amide	H-bonds	holoenzyme only
ribose (ADP)	R44(N)	H-bond (O1′), VDW	
	62–64 backbone	VDW	
	V99	VDW	
2′-PO_4	R44 side chain	ion pair, H-bond	missing in ternary
	S63(Oγ)	H-bonds	
	S64(N,Oγ)	H-bonds	
	Wat-204	H-bond	also H-bonds to R98
pyrophosphate	αC helix	helix dipole	directed at ribose
	αF helix	helix dipole	middle of pyrophosphate
	G95, G96, G97	H-bonds	involves cis peptide
	H45 side chain	ion pair, VDW	
	T46(N,Oγ), H45(N,NE1)	H-bonds	
ribose (NMN) (ternary only)	14–19 backbone	VDW	
	A19(N), E16(O)	H-bonds (O3′)	
	T123	VDW	
	Wat-237	H-bond (O2′)	also H-bonds to folate
nicotinamide (ternary only)	I5, A6	VDW	
	A7(N,O)	H-bonds, (O7, N7)	
	I14(O)	H-bond (N7), dipole (C2)	
	I14, M20 side chains	hydrophobic	
	T46 side chain	VDW, dipole (C6)	
	I94(O)	dipole (C5)	
	G95, G96	VDW	
	Y100(OH)	dipole (C4)	
	folate	VDW	
	Wat-237	dipole (N1)	

[a] VDW, van der Waals contact.

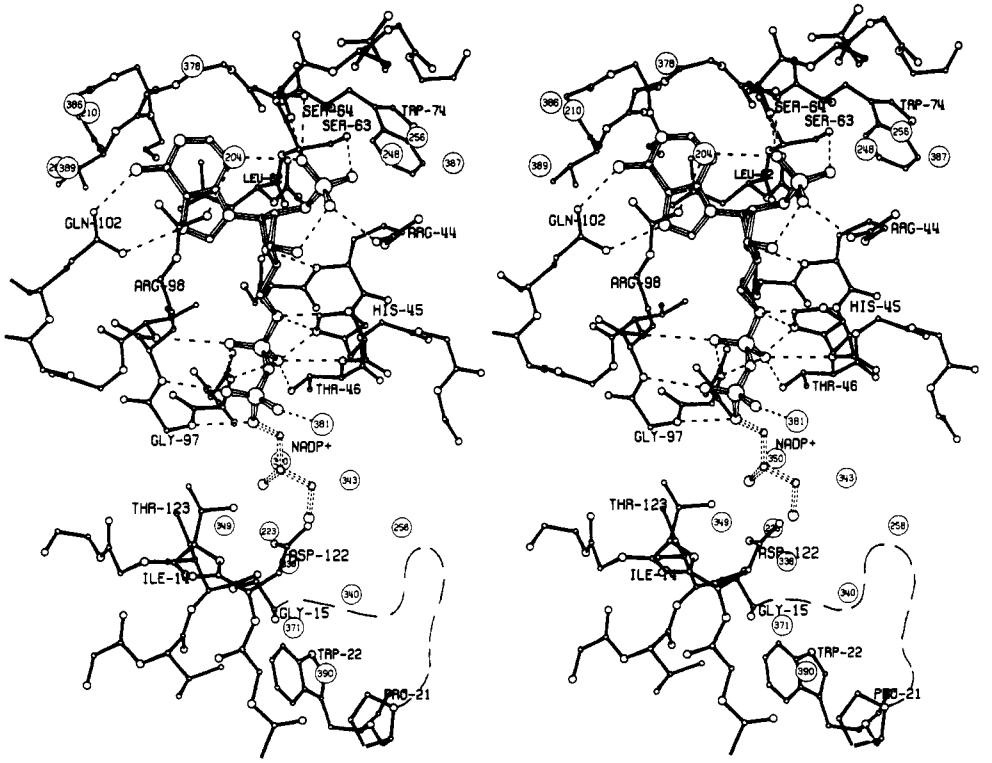

FIGURE 2: $NADP^+$ (striped bonds) bound to DHFR (solid bonds) in the holoenzyme structure. Numbered circles are ordered water molecules. Dashed lines are H-bonds. Partially occupied, disordered portions of the NMN moiety are shown by broken bonds. The curved, dashed line represents the disordered portion (16–20) of the Met-20 loop.

as a basic side chain among all DHFRs and most dehydrogenases, makes a bifurcated H-bond with two oxygens of the ADP group. The side chain of invariant residue Thr-46 also H-bonds to that group. The other seven H-bonds to the pyrophosphate are donated by main-chain nitrogens from the N-termini of αC (residues 45 and 46) and of αF (96, 97, 98, and 99). Gly-96(N) makes a bifurcated H-bond with two oxygens of the ADP 5′-phosphate.

Seven of the ten pyrophosphate H-bonds involve the ADP 5′-phosphate, whereas the NMN phosphate only contributes three H-bonds. The H-bonds from the coenzyme to the αF backbone are greater in number (5) and seem generally to be

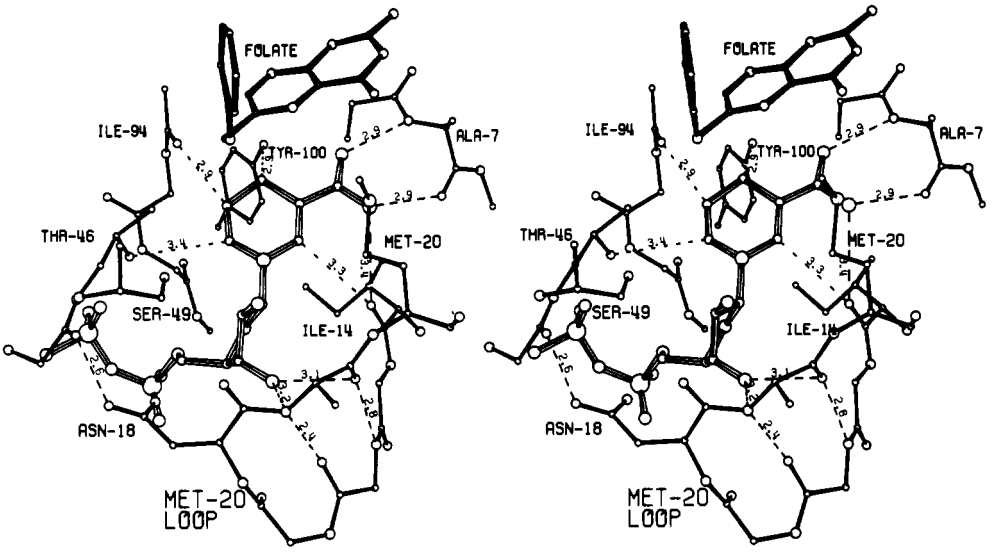

FIGURE 3: Environment of the NMN portion of $NADP^+$ in the folate·$NADP^+$·DHFR ternary complex. $NADP^+$ is shown in striped bonds, folate in boldface solid bonds, and DHFR in lightface solid bonds. Dashed lines indicate distances (not necessarily H-bonds). The Met-20 loop β-turn at the lower right shields the bound NMN from solvent.

somewhat shorter (2.8–3.3 Å) than the H-bonds (2) to the backbone of αC (3.1 and 3.3 Å). Thus the interaction with αF seems to be stronger than the interaction with αC. The αC helix is part of the adenosine binding domain, one of the more mobile parts of the enzyme molecule.

Invariant glycines 95 and 96 form a cis peptide bond which is a conserved feature in all known DHFR structures. This unusual geometry allows Gly-96(N) to insert between two pyrophosphate oxygens while simultaneously making a tight turn from βE to αF. A trans peptide bond between residues 95 and 96 would instead direct the proton on Gly-96(N) away from the phosphates and would probably prevent Gly-96(O) from making an H-bond to Val-99(N).

The ADP 2′-phosphate makes H-bonds to the γ-hydroxyls of serines 63 and 64, Ser-64(N), Wat-204, the side chain of Arg-44, and the 3′-hydroxyl of the adenosine ribose. The latter intramolecular H-bond was not seen in the ternary complex where the 2′-phosphate appears to be rotated about 30° relative to its position in the holoenzyme. (But recall that the high overall temperature factor of the ternary complex structure may render such apparent small differences questionable.) Ser-63 is a conserved hydroxyl side chain, whereas Ser-64 is either a hydroxyl or a basic side chain in known homologous sequences. Arg-44, a conserved basic side chain among known DHFRs, forms an ion pair and an H-bond with the 2′-phosphate. The presence of a basic side chain at this position could account for the 200-fold higher k_{cat}/K_M for NADPH over NADH (Baccanari et al., 1975). NADH-utilizing enzymes usually have an aspartate at this position (Eklund & Branden, 1987).

Interactions with the adenine ring appear to be weaker and less specific than the carefully placed interactions with the phosphates. The side chain of Arg-98 moves about 4 Å from its position in the MTX binary, where it is involved in a lattice interaction, to its location in the holoenzyme, where it stacks with the adenine ring and binds a water (Wat-204) between itself and the 2′-phosphate. In *L. casei* DHFR His-64 plays a role similar to Arg-98 in the *E. coli* enzyme, but from the other side of the binding site. Both close over the bound adenine. The Arg-98 side chain is seemingly attracted by the negative charge of the 2′-phosphate on the opposite side of the binding site. The side chain of Leu-62 forms most of the hydrophobic floor of the adenine binding pocket. Gln-102, in the holoenzyme, H-bonds to N7 and the 6-amino group of the adenine ring forming a Hoogsteen-base-pair-like interaction. But Gln-102, not a conserved residue, is positioned differently in each of the four *E. coli* structures and thus is not likely to provide much selectivity.

The adenosine ribose conformation is 3′-endo, similar to that of the adenosine ribose in the *L. casei* ternary complex. Ribose conformations 3′-endo and 2′-endo are the most common in enzyme-bound NAD(P) molecules (Eklund & Branden, 1987). The adenosine ribose pucker, in this case and for enzyme-bound NADP's in general, is strongly influenced by the manner in which the 2′-phosphate moiety is bound. In this case, the position of the 2′-phosphate is fixed by H-bonding as described above. The position of O3′ is, in turn, fixed by an H-bond to the 2′-phosphate. Thus the enzyme specifically binds the 3′-endo form of the ribose. O1′ of the ribose H-bonds to the backbone nitrogen of Arg-44.

Nicotinamide Mononucleotide (NMN) Binding. The observation of crystallographic disorder in the holoenzyme, reported under Results, confirms ^{31}P NMR studies suggesting that the oxidized NMN moiety of $NADP^+$ is loosely bound, resulting in a broad signal for the 5′-phosphate (Cayley et al., 1980). The same study showed that the reduced NMN of NADPH is more ordered, giving a sharper signal. In consonance with these observations, we have obtained crystals of the NADPH binary complex that are isomorphous with the $P3_221$ folate·$NADP^+$ ternary complex and others of the same space group listed in Table I. If we assume that isomorphous crystals have similar conformations, then we can conclude that the reduced NMN of NADPH in the $P3_221$ form of the holoenzyme is ordered and binds in the same way as the oxidized NMN of $NADP^+$ in the folate·$NADP^+$ ternary complex (Figure 3). This conclusion is not surprising, but it is important in that it allows us to describe the geometry of the Michaelis complex (the dihydrofolate·NADPH·DHFR ternary complex).

A closer look at the pocket that binds the NMN moiety (see Figure 3) reveals that it contains no negatively charged side chains to pair with the positive charge of the oxidized nicotinamide ring, nor are there any aromatic side chains to stack with the aromatic oxidized nicotinamide. It is not surprising therefore that the enzyme binds NADPH, with its uncharged, nonaromatic, reduced nicotinamide ring, about 100 times more tightly than $NADP^+$ (Fierke et al., 1987). In the *L. casei* ternary complex (Filman et al., 1982), oxygen atoms lie close

Table III: Folate Binding Interactions[a]

folate moiety	DHFR atoms	type of interaction	comments
2-amino-4-oxo-pyrimidine	5–7 backbone	VDW	
	I5 side chain	VDW	
	W22 side chain	hydrophobic	
	D27 side chain	H-bonds	conserved acid side chain
	L28 side chain	hydrophobic	conserved hydrophobic side chain
	W30, F31 side chain	hydrophobic	conserved
	Wat-206, -301	H-bonds	W22, T113 involved
pyrazine ring	M20 side chain	VDW	near O4, N5, new
	F31 side chain	hydrophobic	
	I94 side chain	hydrophobic	
	I94(O)	VDW	C7, new, H-bond in MTX·E
	NMN (O7, C4)	VDW	new
PABA	L28, F31, I50, L54	hydrophobic	conserved hydrophobic side chains
	Wat-237	H-bond, N10	new, also H-bonds to NMN
glutamate	K32	VDW, ion pair	γCO_2
	R57 side chain	H-bonds, ion pair	αCO_2, conserved

[a] Abbreviations: MTX·E, methotrexate binary complex; PABA, *p*-aminobenzoic acid; VDW, van der Waals contact. "New" means "not observed in MTX·E".

to carbons 2 and 4–6 in the plane of the nicotinamide ring. As shown in Figure 3, a similar geometry occurs in the present ternary complex; the Tyr-100 hydroxyl, Oγ1 of Thr-46, and the backbone carbonyl oxygens of Ile-14 and Ile-94 are positioned around the perimeter of the pyridine ring. It was proposed that these partial negative charges surrounding the ring stabilize resonance forms with partial positive charges on C2, C4, and C6 of the nicotinamide in the transition state. The carbonyl oxygen of Ile-94 is positioned close to both C5 and C4 of the nicotinamide, but in contrast to the case of the *L. casei* DHFR where they are equidistant from the carbonyl oxygen, C5 is closer to it than C4. This difference may reflect the presence of an additional oxygen, Tyr-100(OH), in the *E. coli* structure. Tyr-100 is invariant in all known DHFR sequences except *L. casei* and *Streptococcus faecium*, where it is replaced by phenylalanine (Volz et al., 1982). In addition to stabilizing a partial positive charge in the transition state, these closely packed oxygens must severely constrain the possible geometries of the nicotinamide ring, allowing the enzyme to select more precisely the subtly altered geometry of the nicotinamide in the transition state, as will be discussed later.

The carboxamide side chain of the nicotinamide is bound to the backbone at Ala-7 with its O7 oxygen held cis to C4. In solution, the lowest energy conformation for the carboxamide has its oxygen trans to C4 of the pyridine ring (Perahia et al., 1975). H-bonds between the carboxamide and the protein backbone at Ala-7 are bent out of the nicotinamide plane toward the side opposite to hydride transfer. This is true in both the *E. coli* DHFR ternary complex and in the *L. casei* DHFR ternary complex. Both the cis conformation of the carboxamide oxygen and the out-of-plane H-bonds to Ala-7 can be interpreted as aiding transition-state binding of the nicotinamide.

Refolding of part of the Met-20 loop (16–19) from a disordered state in the holoenzyme into a type I β-turn in the ternary complex is the most dramatic conformational change seen in these DHFR structures. The importance of the new β-turn in binding the nicotinamide ribose is emphasized by the fact that the *L. casei* DHFR·MTX·NADPH ternary complex (Filman et al., 1982) and the chicken holoenzyme (S. Oatley, unpublished data) both have an analogous β-turn at the same position and by the fact that the binding of NADPH alone causes the refolding. This loop wraps around the bound NMN and binds the 2′-oxygen. In the resulting 2′-endo conformation, O2′ of the nicotinamide ribose helps to bind a water molecule, Wat-237, that sits 3.9 Å above N1 of the nicotinamide ring in the ternary complex (see Figure 7a). Wat-237 is also H-bonded to Oγ of Ser-49 and N10 of folate. The positioning of Wat-237 seems to be important because it could favor the transition state by donating an H-bond to the lone pair of a pyramidalized nicotinamide N1. Although the nicotinamide ring has been shown to be planar in both its oxidized and reduced states (Karle, 1961; Koyama, 1963), the transition state may nevertheless have a pyramidalized N1 (Cook et al., 1981). Since it H-bonds to both folate and $NADP^+$, Wat-237 may bind tightly only when both substrate and coenzyme are also bound.

A similarly positioned water molecule was seen in the *L. casei* DHFR·MTX·NADPH ternary complex, but it cannot be H-bonded to MTX since the latter is methylated at N10. Positioning of a water above N1 is nevertheless possible in the *L. casei* DHFR·MTX·NADPH complex despite the methyl group of MTX because of a shift in position of MTX as compared to folate in the present ternary *E. coli* DHFR structure.

Folate Binding. As expected from the crystal structure of the MTX binary complex (Bolin et al., 1982), folate binds in a deep hydrophobic cleft bisecting the DHFR molecule and containing a single polar residue, Asp-27.

Figure 4 overlays MTX and folate as they bind to superimposed DHFR molecules, but with the enzyme molecules omitted from the figure. As compared with the 2,4-diaminopteridine ring of MTX, the 2-amino-4-oxopteridine ring of folate is rotated roughly 180° about an axis approximately colinear with a line through N5 and NA2 (see Figure 1). The result is that Asp-27 now H-bonds to NA2 and N3 of folate (see Figure 5), rather than NA2 and N1 of MTX. Additionally, C6 is repositioned by 1.9 Å (see Figure 4), and therefore so, too, is the *N*-(*p*-aminobenzoyl)-L-glutamate (PABG) moiety. There is no evidence indicating that the folate pteridine ring binds partially in the "flipped over" manner of MTX, as NMR studies on the *L. casei* DHFR ternary complex have suggested (Birdsall et al., 1989). Two water molecules H-bonded to the pteridine of MTX in the binary complex (Wat-403 and Wat-405) are structurally conserved in the present ternary complex (Wat-206 and Wat-301, see Figure 5).

Table III lists the contacts between folate and the enzyme molecule. Many are the same as between MTX and the enzyme in the binary complex. But notable new interactions with folate are the van der Waals contacts between the pteridine and the $NADP^+$ nicotinamide (behind the pteridine ring in Figure 5), between the Met-20 side chain and the

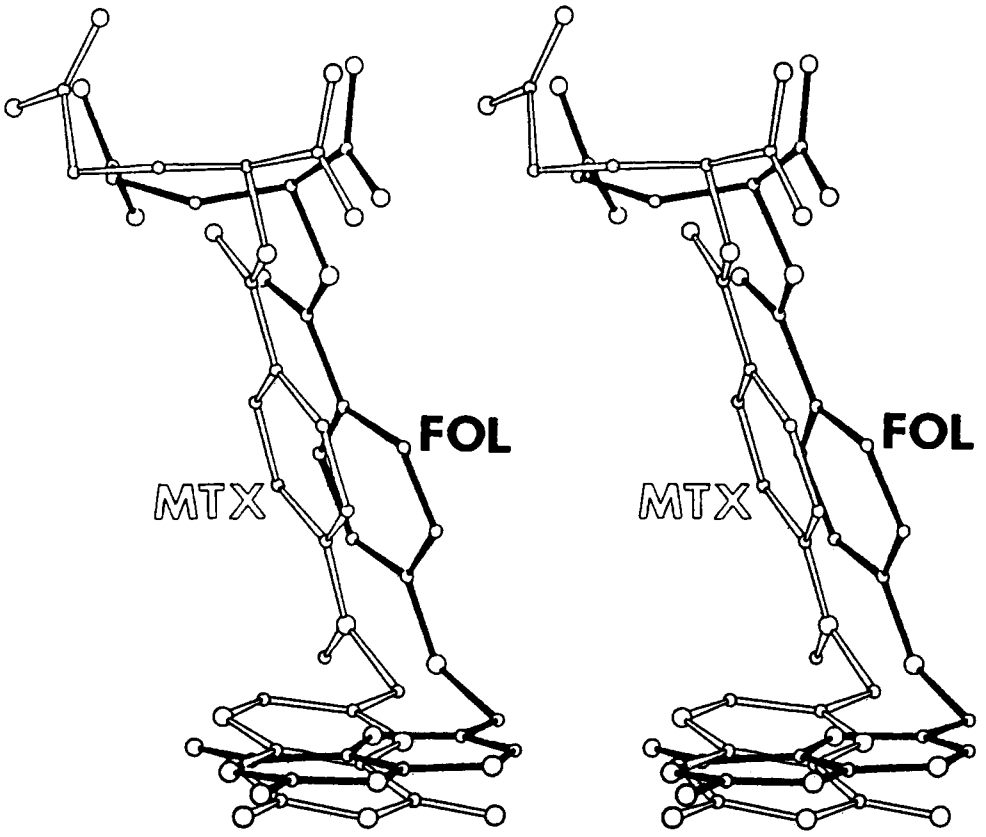

FIGURE 4: Relative positions of MTX (open bonds) and folate (solid bonds) after least-squares superposition of the enzyme molecules in the MTX binary complex (molecule 2) and the folate·$NADP^+$ ternary complex.

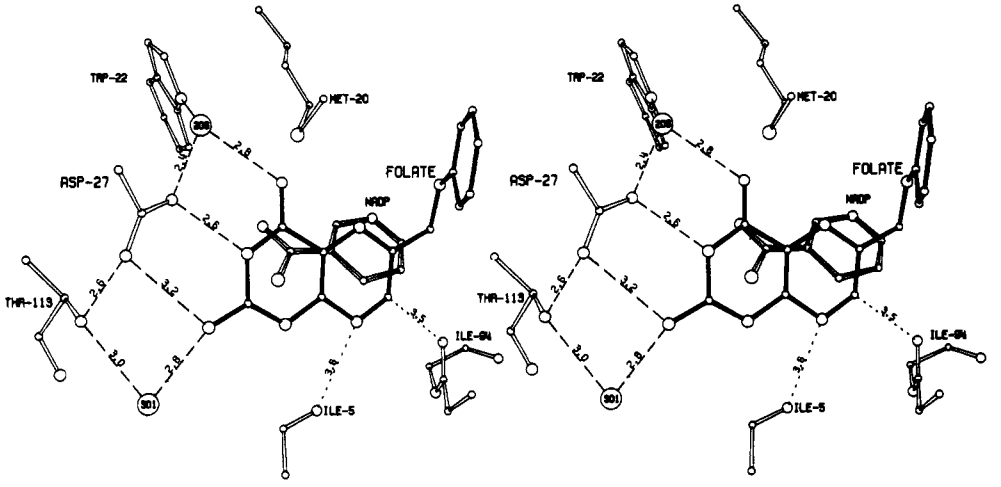

FIGURE 5: Folate (solid bonds) and $NADP^+$ (striped bonds) at the active site of DHFR (open bonds) in the ternary complex. Dashed lines are H-bonds. Dotted lines show non-hydrogen-bonded distances in Å.

pteridine N5 and O4, and between the reoriented pyrazine ring and the backbone at Ile-5 and Ile-94. These new interactions result in an altered positioning of the pteridine ring of folate from what would be predicted by simply flipping over the pteridine ring of MTX by 180°. In Figure 4, one can see that the pteridines of folate and MTX are not coplanar, nor is the axis of rotation relating them exactly collinear with a line through N5 and NA2. The pteridine of folate is twisted about 7° counterclockwise about a perpendicular axis through N3 and is rotated approximately 15° out of the plane of the MTX pteridine about an axis approximately collinear with the C4–C4A bond. It should be noted immediately that an important consequence of these rotations is distortion of the H-bonding to Asp-27.

Role of Asp-27 in Folate Binding. The conserved carboxylate side chain of Asp-27 has at least two distinct functions in catalyzing the reduction of 7,8-dihydrofolate. One is protonation, indirectly, of N5. A second is precisely positioning the dihydropteridine ring by H-bonding. We will take up the issue of protonation later in this discussion, but it should be noted that the ternary complex crystal structure has confirmed our belief that protonation of N5 by Asp-27 cannot be direct.

Although the pteridine ring of folate in the ternary complex is flipped over and rotated as compared with the pteridine ring of MTX in the binary complex (see Figure 4), the side chain of Asp-27 has altered its position only slightly. It moves a little closer to the pteridine and rotates in the opposite direction, clockwise as viewed in Figure 5, such that Oδ2 (the upper oxygen in Figure 5) is shifted back and Oδ1 forward. As a result, the two hydrogen bonds to Asp-27 become quite unequal and are not in the plane of the pteridine. The distance from Asp-27(Oδ2) to N3 is 2.6 Å whereas Asp-27(Oδ1) to

NA2 is 3.2 Å. This distorted H-bonding geometry may contribute to the lower affinity of the enzyme for folate relative to methotrexate, and to its greater specificity for the reduction of dihydrofolate as compared with folate. Folate binds with a dissociation constant around 10^6 times larger than that of MTX (Blakley, 1984). The second-order rate constant (k_{cat}/K_M) for the *E. coli* DHFR catalyzed reduction of dihydrofolate is 2500 times greater than the same parameter for the reduction of folate (Baccanari et al., 1975).

Superposition of all four *E. coli* DHFR structures shows that the Asp-27 side chain shifts only slightly from one to another. The observed differences, as large as 0.6 Å between the ternary and the apoenzyme, are mostly the result of backbone shifts of αB and thus do not imply unusual flexibility of the side chain. On the contrary, Asp-27 has consistently low temperature factors, even in the absence of a bound pteridine (about 19 $Å^2$ in the holoenzyme, 22 $Å^2$ in the apoenzyme), indicating that the side chain is fairly rigid. Thus, by making a pair of H-bonds to its pteridine ring, Asp-27 confers rigidity to the bound substrate. In contrast, the side chain of the equivalent residue, Glu-30, in chicken DHFR is fairly mobile, having only weak density beyond Cγ in the holoenzyme structure (S. Oatley, unpublished observations). Binding of inhibitors such as trimethoprim or phenyltriazine to chicken DHFR causes the side chain of Glu-30 to become more ordered and to shift significantly (Volz et al., 1982). This flexibility may contribute to the increased activity of chicken DHFR toward folate as compared with the *E. coli* enzyme (Kaufman & Gardiner, 1966). The flexibility of Glu-30 in chicken DHFR would allow either C6 (of dihydrofolate) of C7 (of folate) to be positioned above the hydride of the coenzyme without distorting the H-bonds to the carboxylate group. In contrast, the rigidity of Asp-27 in *E. coli* DHFR would disfavor such positioning of C7.

Figure 5 shows the array of H-bonds from folate to Asp-27, two ordered waters (206 and 301), Thr-113, and Trp-22. The H-bonding atoms N1, NA2, and N3 of folate and MTX are sp^2-hybridized, planar-trigonal, and therefore prefer to make H-bonds in the plane of the pteridine ring. In the MTX binary complex, the seven H-bond array [see Figure 8 of Bolin et al. (1982)] is, in fact, approximately planar. But in the folate·$NADP^+$ ternary complex, this H-bond array is significantly distorted from planarity. A careful review of all interactions between the pteridine of folate and the enzyme molecule reveals that distortion of the H-bonds to Asp-27 results from a combination of at least three causes. (1) A shift of the αB helix pushes the side chain of Asp-27 toward the pteridine ring, causing the side chain to twist slightly out of the H-bonding plane. (2) The carbonyl oxygens of Ile-5 and Ile-94 prevent the pteridine from rotating clockwise in the plane to accommodate the shift of the Asp-27 side chain and to regularize the H-bonds, that is, to make the Asp-27(Oδ2)–N3 distance longer and the Oδ1–NA2 distance shorter. (3) Steric interactions between the pteridine and the nicotinamide ring and Phe-31 twist the pteridine out of the H-bonding plane, and in a direction opposing the twist of the Asp-27 side chain.

Asp-27's Role as a Proton Relay. The importance of Asp-27 for substrate protonation has been demonstrated by site-directed mutagenesis experiments in which residue 27 was changed to asparagine or serine (Howell et al., 1986). The activity (k_{cat}/K_M) of the Asn-27 mutant was found to be lower than that of the wild-type enzyme by a factor of 1000 at pH 7.0, while activity–pH profiles indicated that the mutant DHFR rapidly turns over preprotonated substrate but not unprotonated substrate. Thus, the Asp-27 side chain must somehow catalyze substrate protonation at N5. Figure 6 shows how this might occur. In step a to b, the carboxylic acid side chain promotes enolization of the pyrimidine ring by relaying a proton from N3 to O4 via fixed water 206. This step may be assisted by the Gandour effect (Gandour, 1981; see below). In step b to c, we postulate that a temporarily bound water molecule (see below) then H-bonds simultaneously to both O4 and N5. Protonation of N5 by way of this water can be concerted with return of the substrate to the keto form (d). The ultimate source of the net proton gained by the system is the solvent. Note that the Asp-27 side chain is never ionized during this process; indeed if it were ionized, the mechanism would not work, explaining why a protonated carboxylic acid group at this position is required for catalysis (Morrison & Stone, 1988). To speculate somewhat further, it is likely that a requirement for an efficient proton relay is the presence at the Asp-27 site of a group capable of simultaneous protonation and deprotonation at neutral pH. Thus an asparagine side chain in this position cannot promote proton transfer, whereas a serine-bound water molecule, as found in the crystal structure of the Ser-27 mutant (Howell et al., 1986), may do so, albeit inefficiently because of its poor geometry. Indeed, the Ser-27 mutant is 4 times more active than the Asn-27 mutant. It should be noted that, while ionization of Asp-27 is not required by this mechanism, others have proposed that an ionized carboxylate H-bonding to the pyrimidine ring could significantly raise the pK_a of N5 (Gready, 1985).

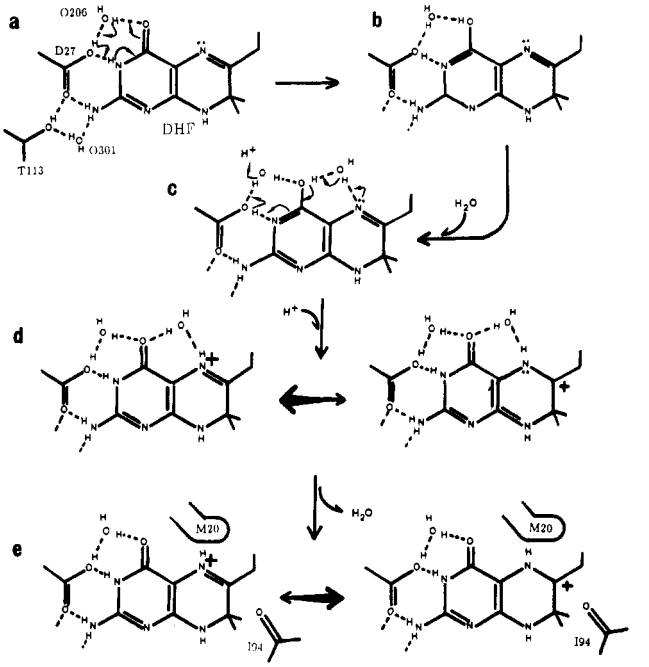

FIGURE 6: (Steps a–d) Proposed mechanism for Asp-27-catalyzed protonation of N5 of 7,8-dihydrofolate. (Step d–e) Proposed catalytic advantage of placing a hydrophobic side chain (Met-20) near the protonated N5.

A question was raised above regarding a possible role for the Gandour effect in this proposed relay mechanism. Gandour (1981) has argued that various lines of evidence indicate that the syn lone pair on a carboxylate oxygen is appreciably more basic than the anti lone pair. Precisely such switching between anti- and syn-bound protons at Oδ2 of Asp-27 is involved in step a to b of Figure 6. In fact, it is possible that the geometry of the hydrogen-bonding network connecting N3, Asp-27, and fixed water 206 may favor the enolic tautomer of the dihydropteridine ring even in the ground-state Michaelis complex. If so, Figure 6d,e should perhaps be represented as an enolic tautomer similar to 6b.

Figure 6d shows two resonance forms of the N5-protonated pyrazine ring. The one on the right, with carbonium ion character at C6, would encourage hydride transfer at C6. (In the transition state C6 should be puckered downward; see later discussion.) Displacement of the temporarily bound water molecule near N5 by the hydrophobic side chain of Met-20, as indicated by step d to e, should favor that resonance form by destabilizing a positive charge at N5, as will be discussed next.

Role of Met-20. The folate·$NADP^+$ ternary complex crystal structure does not show the proposed temporarily bound water molecule between O4 and N5 of the substrate, as depicted in Figure 6c. Instead, we find the side chain of Met-20 occupying that position. But comparisons among the five known *E. coli* DHFR structures have established that Met-20 lies in a very flexible chain segment, so the existence of a hypothetical transient intermediate having an ordered water between O4 and N5 cannot be ruled out. Position 20 (*E. coli* numbering) is conserved as a hydrophobic residue, usually Leu, in all known DHFRs. A possible catalytic advantage of having a hydrophobic side chain handy, ready to occupy a position near N5, is suggested by Figure 6d,e. Recent kinetic investigations have determined, by isotope techniques, that protonation at N5 precedes hydride transfer to C6 (Morrison & Stone, 1988). As depicted in Figure 6e, a hydrophobic group (Met-20) near the N5 end of the protonated N5=C6 double bond and a carbonyl oxygen (Ile-94) near the C6 end ought to favor the resonance form with carbonium ion character at C6. This is precisely what is required to stabilize the transition state for hydride transfer to C6.

Role of Phe-31. The side chain of Phe-31 sits above the pteridine ring, making an aromatic–aromatic interaction and forming an apparently rigid ceiling to the pteridine binding site. The side chain of Phe-31 appears, in fact, to be uncomfortably close to the pteridine ring of folate in the ternary complex. The shortest interatomic distances are about 3.2 Å, whereas the shortest distance to the pteridine of MTX in the binary complex is about 3.6 Å. The difference is caused by the out-of-plane twist of the pteridine of folate, shown in Figure 4. Atoms in equivalent positions in the binding site—N1 and N8 of folate as compared with N3 and NA4 of MTX—are shifted by 0.7 and 0.9 Å, respectively. The Phe-31 side chain also shifts in the ternary complex (about 0.5 Å) but not in precisely the same direction and not by enough to alleviate the crowding. Furthermore, these short contacts cannot be relieved by movement of the pteridine ring away from Phe-31 because of close steric interactions with $NADP^+$ on the opposite side, most importantly between C4 of $NADP^+$ and C6 of folate. Moreover, Phe-31, like Asp-27, exhibits low temperature factors and low conformational variability among the five crystallographically unique *E. coli* DHFR structures. Thus a rigid, precisely defined structure here seems to be important for catalysis. Indeed, mutation of Phe-31 to Val slows hydride transfer by a factor of 6 (Chen et al., 1987).

Role of Carbonyls 5 and 94. The orientation of the backbone carbonyls of Ile-5 and Ile-94 is a conserved feature among the known DHFR crystal structures, although the side chains of these residues are not themselves conserved. Whereas NA4 of MTX makes H-bonds to both backbone carbonyls, folate can H-bond to neither. In the ternary complex, N8 of folate, at a distance of 3.6 Å, is in a position to make an H-bond to Ile-5(O), but has no proton to donate. We have previously pointed out that 7,8-dihydrofolate, with the requisite proton on N8, is likely to make this H-bond [see Figure 8a in Bolin et al. (1982)]. But no H-bonds are possible from the pteridine of folate to Ile-94(O), as the closest pteridine atom is C7, at a distance of 3.5 Å. Additionally, these two backbone carbonyls appear to be positioned so as to interfere with the binding geometry of the folate's pteridine ring. One can see in Figure 5 that a clockwise in-plane rotation of the pteridine to make the H-bonds to Asp-27 equal and both about 2.8 Å would cause the distances from N8 to Ile-5(O) and from C7 (or possibly C9) to Ile-94(O) to become unfavorably short. Furthermore, in the ternary complex, both carbonyl oxygens are already shifted away from the pteridine binding pocket relative to their positions in each of the other complexes. For example, compared to the MTX binary complex, Ile-5(O) is shifted by about 0.5 Å, and Ile-94(O) is shifted by 1.25 Å. Thus, it appears that folate occupies a compromise position, with counterbalancing strains impelling it to move in opposite directions. In contrast, MTX exhibits few unfavorable interactions with the enzyme molecule. The tighter binding of MTX compared to folate can be partly attributed to its favorable interactions (H-bonds) with the carbonyl oxygens of residues 5 and 94, where folate has strained interactions.

Folate/NMN Interactions. Figure 7a shows the immediate vicinity of the pteridine ring and some contact distances between folate, $NADP^+$, and the enzyme molecule. It is apparent that one of the ways in which the enzyme stabilizes the transition state is by forcing C4 of the coenzyme closer to C6 of the substrate. The distance from C4 of the coenzyme to the plane of the pteridine (3.1 Å) is shorter than one would expect for an unstrained contact [about 3.6 Å, based on Chothia (1975)] and even somewhat shorter than the distance used to restrain nonbonded atoms in the refinement process (3.4 Å). The C···H···C distance reported from theoretical studies of transition states for hydride transfers is about 2.6 Å (Wu & Houk, 1987; Donkersloot & Buck, 1981a). Thus, the observed contact distance in the present ternary complex is intermediate between an unstrained van der Waals contact and the theoretical transition-state contact distance. We can see that increasing the C6–C4 distance would force the pteridine closer to the side chain of Phe-31, an already unfavorably close contact at 3.2 Å, and force C4 of the nicotinamide closer to Tyr-100(OH), already strained at 2.8 Å. Additionally, the nicotinamide ring makes contacts with Ile-14(O) and Gly-96(Cα) (distances not shown). The structurally conserved orientation of the latter is a result of the conserved 95–96 cis peptide bond. These contacts, and that with the side chain of Ile-14 (not shown), combine to prevent the nicotinamide ring from moving downward (as viewed in Figure 7a) to relieve the close contact with folate. But if we further *shortened* the C4···C6 distance, as would happen in the transition state for hydride transfer between those two carbons, many of these unfavorably short contacts could be relieved.

PABG Binding. The (*p*-aminobenzoyl)-L-glutamate (PABG) tail of folate binds in a hydrophobic pocket surrounded by the side chains of Leu-28, Phe-31, Ile-50, and Leu-54 (see Figure 7). The α-carboxyl group of the glutamate makes an ion pair and two H-bonds to invariant residue Arg-57. The angle between the plane of the *p*-aminobenzoyl ring and the pteridine ring is 75°, rather than the almost 180° seen in the crystal structure of folic acid itself (Mastropaolo et al., 1980). As a result, C15 in the benzene ring is brought within 3.1 Å of C6, somewhat shorter than a usual van der Waals contact [3.6 Å, based on Chothia (1975)]. This strained contact may favor a transition state in which the whole PABG tail extends further away from C6, allowing the C6···C15 distance to increase. Such an upward shift of the tail relative

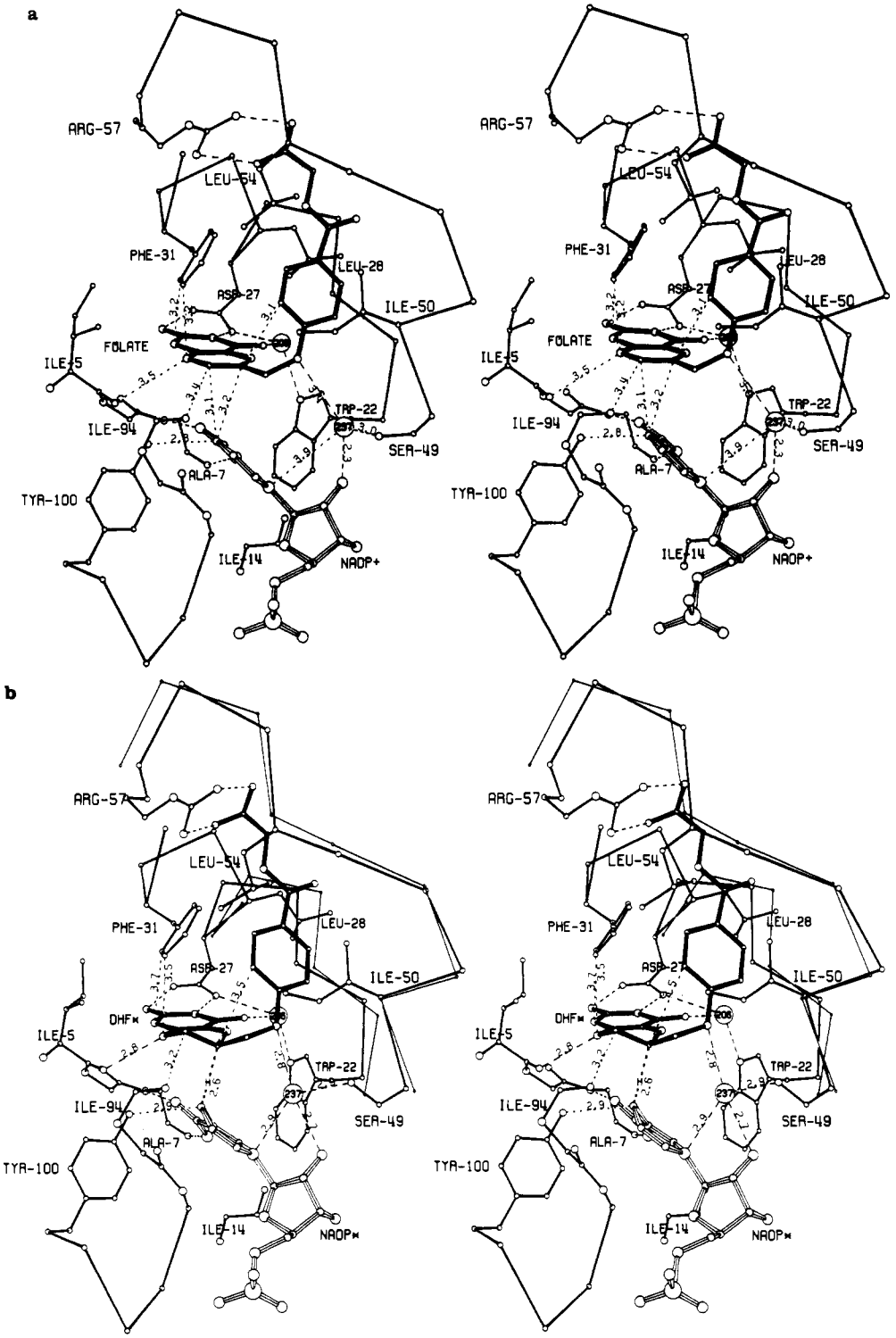

FIGURE 7: (a) Active site of folate·$NADP^+$ ternary complex, showing some of the contacts discussed in the text. Folate is shown in boldface solid bonds, $NADP^+$ in striped bonds, and DHFR in lightface solid bonds. (b) Hypothetical transition-state complex. Thin-line bonds show the crystallographically observed α-carbon positions in the ternary complex where the enzyme conformation was changed in the model.

to the pteridine ring is expected when C6 goes from planar-trigonal to pyramidal in the transition state.

The position of the PABG tail of folate in the ternary complex is displaced about 1.3 Å from the position of the PABG of MTX in the binary complex. This difference is correlated with reversal of the pteridine ring, which puts the PABG moiety of folate closer to the side chains of Phe-31, Ile-50, and Leu-54 and farther away from Leu-28. Conformational changes partially accommodate the shift, but interactions with the enzyme molecule impel the PABG to bend back toward its position in the MTX binary complex. The bending of the PABG to make a more acute angle with the pteridine ring and the in-plane counterclockwise rotation of the pteridine ring also serve to displace the PABG toward the MTX position. Barriers preventing further such displacement of the tail are distorted H-bonding to Asp-27 and the contact between C15 and C6 (3.1 Å) caused by the acute tail angle (see Figure 7a).

Model Building Studies: *The Michaelis Complex*. On the basis of the crystallographically observed folate·$NADP^+$ ternary complex described above, we have modeled a hypothetical dihydrofolate·NADPH·DHFR complex, i.e., the Michaelis

complex, and a hypothetical transition-state complex. The region that was rebuilt is shown in Figure 7; the observed folate·$NADP^+$ ternary complex is depicted in Figure 7a and the hypothetical transition state complex in Figure 7b.

In arriving at these models, we have assumed that the reduced nicotinamide moiety of NADPH binds with the same geometry as the oxidized nicotinamide of $NADP^+$. Only Wat-237, above the nicotinamide N1, has been adjusted slightly to make more idealized H-bonds. Nor were any changes made from the observed geometry of the ternary complex in the vicinity of the bound ADP moiety, even though some such changes probably do occur.

Such changes as were made in the enzyme molecule's geometry at the dihydrofolate binding site are consistent with conformational variability actually observed among the five crystallographically independent *E. coli* DHFR structures. In essence, 7,8-dihydrofolate differs from folate only in that the former has an attached hydrogen atom at N8 and an additional hydrogen atom attached to C7 and the partly reduced pyrazine ring is more flexible. The crystal structure of 7,8-dihydropterin (Bieri, 1977) suggests that the 7,8-dihydropyrazine ring of dihydrofolate remains planar in its lowest energy conformation. We therefore assumed it to be planar in constructing a model of the Michaelis complex. Our initial premise in modeling bound dihydrofolate was that N8 donates an H-bond to Ile-5(O). All other structural adjustments were a consequence of minimizing the resulting unfavorable contacts while conserving favorable ones. In particular, conserving the interaction between the PABG αCO_2 moiety and Arg-57 required significant displacements of some enzyme groups.

When modeling a hydrogen bond between N8 of the 7,8-dihydropteridine ring and the carbonyl oxygen of Ile-5, the distance between N8 and Ile-5(O) must be shortened, causing a clockwise 7° in-plane rotation of the pteridine ring relative to its orientation in the observed folate-containing ternary complex. This rotation would position C6 of dihydrofolate close to the ideal geometrical relationship with the nicotinamide for transfer of a hydride from C4 of the latter. It would also allow the distorted H-bonds between the pteridine ring and Asp-27 to approach their normal geometry. Wat-206, H-bonded to O4 of the dihydropteridine, can also move to accommodate this rotation without sacrificing good H-bonding geometry to Trp-22 and Asp-27. However, this hypothetical rotation of a rigidly planar pteridine ring would put C7 too close to Ile-94(O), at a distance of about 3.1 Å. Since Ile-94(O) is below the plane of the ring, C7 will be encouraged to pucker upward, out of plane. Such an enforced upward puckering at C7, accompanied by a downward puckering at C6, would contribute to transition-state stabilization (see below).

Close inspection of the geometrical differences between folate binding and our model for dihydrofolate binding suggests at least one reason behind the enzyme's preference for dihydrofolate over folate as a substrate. Simply put, in the folate-containing ternary complex C7 of folate is not positioned with respect to the nicotinamide for efficient hydride transfer. Instead, the relative orientation of the would-be reactants is such that a hydride coming from C4 of the coenzyme is directed at a point midway between C6 and C7 of folate. Note that rotating the pteridine ring of folate so that the hydride points directly at C7 would further distort the H-bonds to Asp-27. This less-than-ideal binding geometry of folate reflects its minimal turnover by the *E. coli* enzyme, $^1/_{2500}$ that of dihydrofolate in terms of relative second-order rate constants, k_{cat}/K_M (Baccanari et al., 1975).

The PABG tail position for dihydrofolate was modeled to accommodate the rotation of the dihydropteridine ring just described. Hydrogen-bonded interactions between the αCO_2 and the side chain of Arg-57 were assumed to be conserved in the Michaelis complex. The C6–C9, C9–N10, and N10–C11 torsion angles were modified to place the benzoyl ring at a reasonable van der Waals contact distance from Phe-31. Other contact distances were optimized by shifting enzyme groups on either side of the PABG binding crevice according to the observed flexibility of those regions of the molecule. In its resulting position, the PABG moiety occupies roughly the same space as it does in the observed ternary complex but is tilted with respect to the PABG of folate, with its glutamate end shifted toward the Leu-28 side of the pocket.

Model Building Studies: The Transition-State Ternary Complex. Figure 7b shows our proposed model of the transition state for DHFR-catalyzed hydride transfer. The essential changes from the model of the dihydrofolate·NADPH ternary complex are a shorter distance from C6 of the dihydropteridine to C4 of the nicotinamide (2.6 Å), a change in the geometry at C6 of the dihydropteridine ring from planar-trigonal to pyramidal, and a change in the conformation of the nicotinamide ring consistent with theoretical studies of the transition state for hydride transfer (see below). As for the modeling of the Michaelis complex, described above, minimizing unfavorable interactions and conserving the interaction with Arg-57 required making further adjustments to the enzyme molecule. We think it is most intriguing that, in doing so, we found that an enzyme conformation approaching that seen in the MTX binary complex fits the transition state quite well. This observation leads to speculation on the reasons for the very tight binding of this inhibitor and raises questions about whether MTX might in some ways resemble a transition-state analogue.

Modeling of the nicotinamide in the transition-state complex was based on a consensus of information from theoretical and model building studies. Theoretical studies on hydride transfer from 1,4-dihydronicotinamide (Donkersloot & Buck, 1981a,b) suggest that, in the optimal transition state, C4 of the nicotinamide is puckered slightly out of the plane of the ring in the direction of hydride transfer; C7, the carboxamide carbon, is bent slightly out of plane away from the hydride-transfer direction; and the carboxamide oxygen is cis to C4. Our present model building studies suggest that, by shifting C4 out of plane in the direction of hydride transfer, we partially relieve an unfavorably close contact between C4 and Tyr-100(OH). In the crystallographically observed ternary complex, the OH···C4 distance is 2.8 Å and the Tyr-100 hydroxyl itself is strained in the direction of the nicotinamide by a short H-bond (2.3 Å) to Ile-5(O) (not shown in Figure 7). In our transition-state model, the unfavorable contact between Tyr-100-(OH) and C4 has been relaxed somewhat to 3.0 Å. An unstrained contact distance would be 3.2 Å (Chothia, 1975). The carboxamide moiety of $NADP^+$ makes two slightly out-of-plane H-bonds to the backbone at Ala-7. Bending the carboxamide out of the nicotinamide plane toward Ala-7 in the transition state would optimize the geometry of these H-bonds. The same bending would also partially alleviate a close contact between the carboxamide O7 and C8A of the substrate.

Experimental evidence suggests that N1 of the nicotinamide may be pyramidalized in the transition state of liver alcohol dehydrogenase (Cook et al., 1981). In our model, we have partially pyramidalized N1 by slightly rotating the whole pyridine ring about an axis through C3 and C5 while keeping the ribose fixed. Support for this means of pyramidalizing

N1 comes from the theoretical studies cited earlier (Donkersloot & Buck, 1981b) suggesting that, in the transition state, N1 remains within the plane of the 1,4-dihydronicotinamide ring but that its attached hydrogen (equivalent to C1′ of the ribose) shifts out of plane away from hydride transfer. C1′ should therefore be modeled below the plane. In the case of enzyme-bound NADPH, slightly rotating the nicotinamide to model the transition state with a pyramidalized N1 is preferred over adjusting the ribose as the latter would involve more drastic shifting of enzyme groups.

The transition state of the dihydropteridine ring was built into the substrate binding site in a geometry that best relieves unfavorable contacts in our model of the dihydrofolate·NADPH Michaelis complex. C7 of the pyrazine ring is above the plane and C6 is below the plane. Puckering C6 downward combined with an upward puckering of the nicotinamide C4 (as viewed in Figure 7b) shortens the distance between them to 2.6 Å, the theoretical carbon–carbon distance for the hydride-transfer transition state (Wu & Houk, 1987). Also, when C7 puckered upward, the close contact between that atom and Ile-94(O) was lengthened to 3.3 Å. Modeling C7 as far out of plane as we have is consistent with energy-minimization studies, where out-of-plane shifts of more than 0.5 Å have been predicted for C7 in 5,6,7,8-tetrahydropterin (Gready, 1984).

In modeling the transition state, we made no additional in-plane rotations of the dihydropteridine ring beyond those already made in modeling ground-state dihydrofolate binding. Nevertheless, the H-bonds from the pteridine to Asp-27 may improve further in the transition state as a result of a shift of the αB helix resulting from a change in the PABG tail conformation. Specifically, the H-bonds to Asp-27 are likely to become more nearly equal and more coplanar with the pteridine ring.

Our model for PABG binding in the transition state was constructed by continuing the process used for modeling PABG in the Michaelis complex. The Arg-57/αCO_2 interaction was conserved, and contacts with the hydrophobic side chains of residues 28, 31, 50, and 54 were optimized. The essential difference between the PABG tail position in the Michaelis complex model and the transition-state model is a shift of about 0.2 Å along the long axis of the tail, resulting from the change in the geometry at C6 from planar to pyramidal. Although small, this shift relieves a close van der Waals contact between C15 of the benzoyl ring and C6 of the pteridine.

ACKNOWLEDGMENTS

We thank our colleagues J. F. Davies, J. Wang, J. T. Hirai, and M. F. Farnum, for helpful discussions and criticisms. We acknowledge a generous grant of CPU time on the San Diego Supercomputer, without which this project would not have been possible.

Registry No. DHFR, 9002-03-3; 7,8-dihydrofolate, 4033-27-6.

REFERENCES

Anderson, D. H. (1987) Ph.D. Thesis, University of California, San Diego, La Jolla, CA.

Baccanari, D., Phillips, A., Smith, S., Sinski, D., & Burchall, J. (1975) *Biochemistry 14*, 5267–5273.

Benkovic, S. J., Fierke, C. A., & Naylor, A. M. (1988) *Science 239*, 1105–1110.

Bieri, J. H. (1977) *Helv. Chim. Acta 60*, 2303–2308.

Birdsall, B., Feeney, J., Tendler, S. J. B., Hammond, S. J., & Roberts, G. C. K. (1989) *Biochemistry 28*, 2297–2305.

Blakley, R. L. (1984) in *Folates and Pterins, Vol. 1, Chemistry and Biochemistry of Folates* (Blakley, R. L., & Benkovic, S. J., Eds.) pp 191–253, John Wiley & Sons, New York.

Blakley, R. L., & Appleman, J. R. (1986) in *Chemistry and Biology of Pteridines*, pp 769–788, de Gruyter, New York.

Bolin, J. T., Filman, D. J., Matthews, D. A., Hamlin, R. C., & Kraut, J. (1982) *J. Biol. Chem. 257*, 13650–13662.

Bystroff, C. (1988) Ph.D. Thesis, University of California, San Diego, La Jolla, CA.

Cayley, P. J., Feeney, J., & Kimber, B. J. (1980) *Int. J. Biol. Macromol. 2*, 251–255.

Champness, J. N., Stammers, D. K., & Beddell, C. R. (1986) *FEBS Lett. 199*, 61–67.

Chen, J. T., Taira, K., Tu, C. P. D., & Benkovic, S. J. (1987) *Biochemistry 26*, 4093–4100.

Chothia, C. (1975) *Nature 254*, 304–308.

Cook, P. F., Oppenheimer, N. J., & Cleland, W. W. (1981) *Biochemistry 20*, 1817–1825.

Cork, C., Fehr, D., Hamlin, R., Vernon, W., Xuong, N.-H., & Perez-Mendez, V. (1973) *J. Appl. Crystallogr. 7*, 319–323.

Crowther, R. A. (1972) in *The Molecular Replacement Method* (Rossmann, M. G., Ed.) pp 173–178, Gordon and Breach, New York.

Crowther, R. A., & Blow, D. M. (1967) *Acta Crystallogr. 23*, 544–548.

Dempsey, S. (1987) *Molecular Modeling System* (MMS), Department of Chemistry Computer Facility, University of California, San Diego, La Jolla, CA.

Donkersloot, M. C. A., & Buck, H. M. (1981a) *J. Am. Chem. Soc. 103*, 6549–6554.

Donkersloot, M. C. A., & Buck, H. M. (1981b) *J. Am. Chem. Soc. 103*, 6554–6558.

Eklund, H., & Branden, C.-I. (1987) in *Pyridine Nucleotide Coenzymes* (Dolphin, D., Poulson, R., & Avramovic, O., Eds.) Vol. 2, Part A, pp 51–98, John Wiley & Sons, New York.

Fierke, C. A., Johnson, K. A., & Benkovic, S. J. (1987) *Biochemistry 26*, 4085–4092.

Filman, D. J., Bolin, J. T., Matthews, D. A., & Kraut, J. (1982) *J. Biol. Chem. 257*, 13663–13672.

Gandour, R. D. (1981) *Bioorg. Chem. 10*, 169–176.

Gready, J. E. (1984) *J. Mol. Struct.: THEOCHEM. 109*, 231–244.

Gready, J. E. (1985) *Biochemistry 24*, 4761–4766.

Hendrickson, W. A. (1985) *Methods Enzymol. 115*, 252–270.

Howell, E. E., Villafranca, J. E., Warren, M. S., Oatley, S. J., & Kraut, J. (1986) *Science 231*, 1123–1128.

Howell, E. E., Warren, M. S., Booth, C. L. J., Villafranca, J. E., & Kraut, J. (1987) *Biochemistry 26*, 8591–8598.

Jones, T. A. (1978) *J. Appl. Crystallogr. 11*, 268–272.

Karle, I. L. (1961) *Acta Crystallogr. 14*, 497–502.

Kaufman, B. T., & Gardiner, R. C. (1966) *J. Biol. Chem. 241*, 1319–1328.

Koyama, H. (1963) *Z. Krystallogr. 118*, 51–68.

Kraut, J., & Matthews, D. A. (1987) in *Biological Macromolecules and Assemblies* (Jurnak, F. A., & McPherson, A., Eds.) Vol. 3, pp 1–72, John Wiley & Sons, New York.

Leslie, A. G. W. (1985) in *Proceedings of the Daresbury Study Weekend*, pp 78–81, Daresbury Laboratory, Daresbury, Warrington, England.

Luzzatti, V. (1952) *Acta Crystallogr. 5*, 802–810.

Mastropaolo, D., Camerman, A., & Camerman, N. (1980) *Science 210*, 334–336.

Matthews, D. A., Alden, R. A., Bolin, J. T., Freer, S. T., Hamlin, R., Xuong, N.-H., Kraut, J., Poe, M., Williams, M., & Hoogsteen, K. (1977) *Science 197*, 452–455.

Matthews, D. A., Bolin, J. T., Burridge, J. M., Filman, D. J., Volz, K. W., Kaufman, B. T., Beddell, C. R., Champness, J. N., Stammers, D. K., & Kraut, J. (1985) *J. Biol. Chem. 260*, 381-391.

Morrison, J. F., & Stone, S. R. (1988) *Biochemistry 27*, 5499-5506.

Perahia, D., Pullman, B., & Saran, A. (1975) in *Structure and Conformation of Nucleic Acids and Protein-Nucleic Acid Interactions* (Sundadlingam, M., & Rao, S. T., Eds.) pp 685-708, University Park Press, Baltimore.

Rossmann, M. G., & Argos, P. (1975) *J. Biol. Chem. 250*, 7525-7532.

Sussman, J. L., Holbrook, S. R., Church, G. M., & Kim, S.-H. (1977) *Acta Crystallogr. A33*, 800-804.

Tanaka, N. (1977) *Acta Crystallogr. A33*, 191-193.

Villafranca, J. E., Howell, E. E., Voet, D. H., Strobel, M. S., Ogden, R. C., Abelson, J. N., & Kraut, J. (1983) *Science 222*, 782-788.

Volz, K. W., Matthews, D. A., Alden, R. A., Freer, S. T., Hansch, C., Kaufman, B. T., & Kraut, J. (1982) *J. Biol. Chem. 257*, 2528-2536.

Wang, J., Mauro, J. M., Fishel, L. A., Edwards, S. L., Xuong, N.-H., Ashford, V., & Kraut, J. (1990) *Biochemistry* (in press).

Wu, Y.-D., & Houk, K. N. (1987) *J. Am. Chem. Soc. 109*, 2226-2227.

Xuong, N.-H., Neilson, C., Hamlin, R., & Anderson, D. H. (1985) *J. Appl. Crystallogr. 18*, 342-350.

^{1}H NMR Sequential Assignments and Secondary Structure Analysis of Human Fibrinogen γ-Chain C-Terminal Residues 385-411†

K. H. Mayo* and C. Burke

Department of Chemistry, Temple University, Philadelphia, Pennsylvania 19122

J. N. Lindon

Beth Israel Hospital, Harvard Medical School, Boston, Massachusetts 02155

M. Kloczewiak

Burns Institute, Shriners Hospital for Crippled Children, Boston, Massachusetts 02114

Received August 1, 1989; Revised Manuscript Received November 1, 1989

ABSTRACT: The human fibrinogen γ-chain, C-terminal fragment, residues 385-411, i.e., KIIPFNRLTIGEGQQHHLGGAKQAGDV, contains two biologically important functional domains: (1) fibrinogen γ-chain polymerization center and (2) platelet receptor recognition domain. This peptide was isolated from cyanogen bromide degraded human fibrinogen and was investigated by ^{1}H NMR (500 MHz) spectroscopy. Sequence-specific assignments of NMR resonances were obtained for backbone and side-chain protons via analysis of 2D NMR COSY, double quantum filtered COSY, HOHAHA, and NOESY spectra. The N-terminal segment from residues 385-403 seems to adopt a relatively fixed solution conformation. Strong sequential αCH-NH NOESY connectivities and a continuous run of NH-NH NOESY connectivities and several long-lived backbone NH protons strongly suggest the presence of multiple-turn or helix-like structure for residues 390 to about 402. The conformation of residues 403-411 seems to be much less constrained as evidenced by the presence of weaker and sequential αCH-NH NOEs, the absence of sequential NH-NH NOEs, and the lack of longer lived amides. Chemical shifts of resonances from backbone and side-chain protons of the C-terminal dodecapeptide, residues 400-411, differ significantly from those of the parent chain, suggesting that some preferred C-terminal conformation does exist.

The vertebrate fibrinogen molecule (330000 daltons) in its native form is a dimer, each half-molecule being composed of three nonidentical polypeptide chains (α, β, and γ) (Blomback & Yamashina, 1958). Its transformation into fibrin is a self-assembly process following thrombin-catalyzed removal of fibrinopeptides from the amino termini of the α- and β-chains. The fibrinogen chains can be chemically cross-linked between two α-chains (McKee et al., 1970) and between two γ-chains (Chen & Doolittle, 1969), presumably through ε-amino(γ-glutamyl)lysine bonds (Chen & Doolittle, 1970). The C-terminal γ-chain fragment of residues 392-411 was identified as being responsible for the γ-γ chain cross-linking/polymerization (Chen & Doolittle, 1971). Doolittle (1973) modeled this segment in an α-helix structure to hypothesize cross-linking sites between γ-chains.

More recently, Kloczewiak et al. (1982) showed that the domain recognizing receptors on ADP-activated human platelets is located on the human fibrinogen γ-chain between residues 385 and 411 which when cleaved to the smaller fragment, residues 400-411, maintains nearly full biological activity (Kloczewiak et al., 1984). Substitution of one amino acid for another in this dodecapeptide fragment can greatly affect its activity (Ruggeri et al., 1986; Kloczewiak et al., 1988), suggesting that either a specific (sequence of) residue(s) or a specific backbone folding pattern or both is necessary for activity.

Due to the biological significance of the fibrinogen γ-chain C-terminal fragment, we chose to investigate the solution conformation of γ-chain residues 385-411 by using two-dimensional (2D)[1] proton NMR spectroscopy. In this study,

†This work was supported by a grant from the W. W. Smith Charitable Trust and benefited from NMR facilities made available to Temple University through Grant RR-04040 from the National Institutes of Health (to K.H.M.).

*Author to whom correspondence should be addressed.

0006-2960/90/0429-3277$02.50/0